Catalyst-Free Growth and Characterization of ZnO Nanorods

Jih-Jen Wu* and Sai-Chang Liu

Department of Chemical Engineering, National Cheng Kung University, Tainan 701, Taiwan

Received: April 19, 2002; In Final Form: June 13, 2002

Highly oriented ZnO nanorods have been grown on various substrates, such as fused silica, Si(100), and sapphire (110), using a simple catalyst-free CVD method at low temperatures. TEM analyses indicate that epitaxial ZnO nanorods have been grown on sapphire (110) with the ZnO/sapphire orientational relationship [001]||[110] and [110]||[001]. In the Si(100) substrate, an amorphous SiO_x interfacial layer exists between ZnO nanorods and Si(100). The well-aligned ZnO nanorods on fused silica substrates exhibit a strong UV emission and absorption at around 386 nm under room temperature. Photoluminescence and Raman spectra indicate that there is a very low concentration of oxygen vacancies in the highly oriented ZnO nanorods. Diameter control of the well-oriented and high-quality ZnO nanorods is achievable by variation of the growth conditions.

Introduction

One-dimensional (1-D) nanometer-sized semiconductor materials have attracted considerable research activities because of their great potential for fundamental studies of the roles of dimensionality and size in their physical properties as well as for applications in optoelectronic nanodevices and functional materials.[1] ZnO is a versatile material and has been used considerably for its catalytic, electrical, optoelectronic, and photochemical properties.[2] Recently, room-temperature UV lasing properties[3] in ZnO epitaxial films, microcrystalline thin films, and nanoclusters have stimulated intensive interest in the optical properties of ZnO. ZnO exhibits a hexagonal structure with a direct band gap of 3.37 eV at room temperature, which is very similar to that of GaN. Moreover, ZnO possesses a large exciton binding energy of 60 meV. The strong exciton binding energy which is much larger than that of GaN (25 meV) as well as the thermal energy at room temperature (∼26 meV) can ensure an efficient exciton emission at room temperature.[4] The synthesis of one-dimensional ZnO nanostructures has also been of growing interest owing to the promising application in nanoscale optoelectronic devices. The growth of 1-D single-crystalline ZnO nanostructures have been demonstrated by various high-temperature processes, such as vapor−liquid−solid (VLS) growth mechanism (≥900 °C)[5] and thermal evaporation (1400 °C).[6] Room-temperature UV lasing in ZnO nanowires has been demonstrated very recently.[7] However, for practical application, low-temperature growth of high-quality and well-ordered 1-D ZnO nanostructures with controlled diameters will be required.

In comparison with those processes which were carried out at rather high temperatures, ZnO nanorods have been formed through simple thermal reaction of zinc acetylacetonate and oxygen at low temperatures.[8] In this work, low-temperature growth of ZnO nanorods on various substrates is investigated using this catalyst-free CVD process. Highly oriented ZnO nanorods are grown on fused silica, Si(100), and sapphire (110). The well-aligned ZnO nanorods exhibit a strong UV emission and absorption at around 386 nm under room temperature. TEM analyses indicate that epitaxial ZnO nanorods are grown on sapphire (110). Furthermore, diameter-controlled growth of well-oriented and high-quality ZnO nanorods on fused silica substrates is achieved using the catalyst-free and low-temperature CVD approach. We believe the presented approach is a simple one for practical application of ZnO nanostructures to optoelectronic devices.

Experimental Section

ZnO nanorods were grown in a 3″ quartz tube insert to a two-temperature-zone furnace. The quartz tube was well-sealed for being able to maintain a base pressure of 5.0×10^{-3} Torr. Zinc acetylacetonate hydrate ($Zn(C_5H_7O_2)_2 \cdot xH_2O$, Lancaster, 98%), which was employed to be zinc source, placed on a cleaned Pyrex glass container was loaded into the low-temperature zone of the furnace. The temperature was controlled to be at 130−140 °C to vaporize the solid reactant. The vapor was carried by a N_2/O_2 flow into the higher temperature zone of the furnace in which substrates were located. Fused silica, Si(100), sapphire (001), and sapphire (110) were employed as substrates for ZnO nanorods growth. They were cleaned in an ultrasonic bath of acetone for 20 min and Si(100) substrates were further dipped in HF solution and DI water before being loaded into the quartz tube. There is no catalytic metal film precoated on these substrates. The total pressure of the quartz tube was 200 Torr during ZnO nanorod growth.

The morphology and size distribution as well as elemental analyses of the nanorods were examined using scanning electron microscopy (SEM, Hitachi, S-4200) equipped with energy dispersive spectrometry (EDS). A high-resolution (HR) SEM (JEOL, JSM-6700F) was also employed to study the detailed morphology of the ZnO nanorods. The crystal structure of the nanorods was analyzed using X-ray diffraction (XRD, Rigaku D/MAX-2000) and high-resolution transmission electron microscopy (HRTEM, JEOL, JEM-4000EX). Electron energy-loss spectroscopy (EELS, GIF 2000) equipped on a TEM (Philips Tecnai 20) was employed to analyze the qualitative compositions of the products. Photoluminescence studies were conducted using a Hitachi F-4500 fluorescence spectrophotometer with a

* To whom correspondence should be addressed. E-mail: wujj@mail.ncku.edu.tw.

10.1021/jp025969j CCC: $22.00
Published on Web 08/17/2002

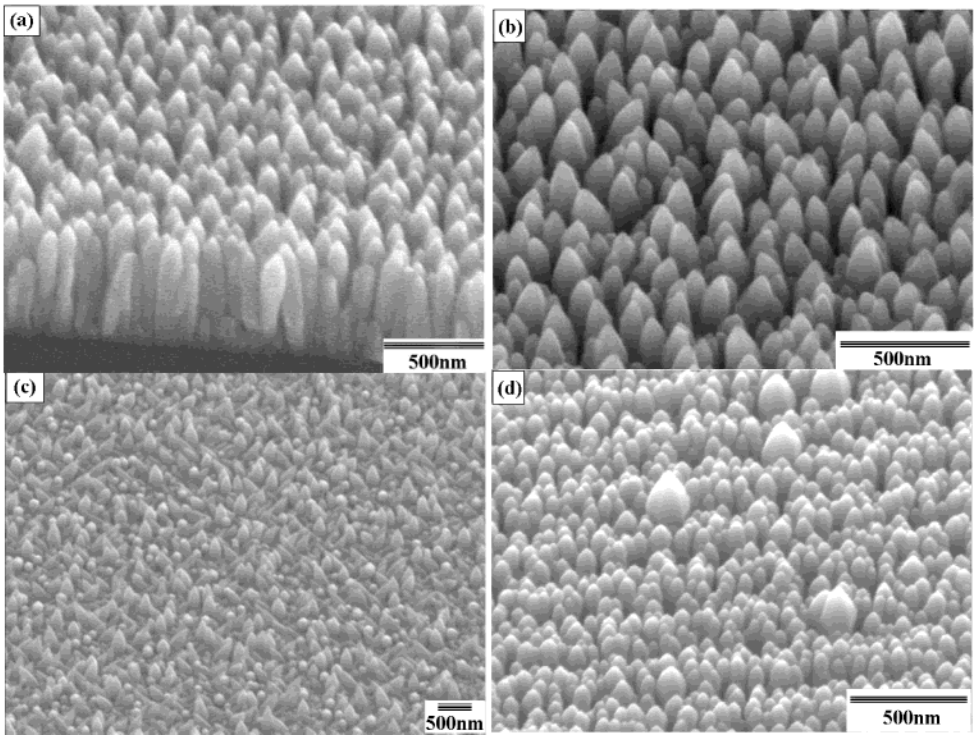

Figure 1. SEM images of ZnO nanorods grown on (a) fused silica, (b) Si(100), (c) sapphire (001), and (d) sapphire (110).

Xe lamp at room temperature. The excitation wavelengths were 325 nm. The optical absorption spectra were measured using a Jasco V-500 UV/vis spectrophotometer with a deuterium discharge tube (190−350 nm) and a tungsten iodine lamp (330−900 nm). The Raman spectra were recorded on a Renishaw system 2000 micro-Raman spectrometer with a 514.5 nm Ar^+ laser as an excitation source.

Results and Discussion

Effects of Substrate Materials on ZnO Nanorod Growth. To study the effects of substrate materials on the growth of highly oriented ZnO nanorods, four types of materials, including fused silica, Si(100), sapphire (001), and sapphire (110), are chosen as substrates for the growth of ZnO nanorods at a vaporizing temperature of 135 °C, a N_2/O_2 flow rate of 250/250 sccm, and a substrate temperature of 500 °C. Among them, sapphire (001) and (110) have been employed to be the substrates for epitaxial growth of ZnO films.[9] The SEM images of the ZnO nanorods grown on those substrates are shown in Figure 1. In the ZnO nanorods grown on the fused silica and the Si(100) substrates, a high density of well-oriented nanorods uniformly grew over the entire substrate. The diameter and the length of the nanorods were in the ranges of 60−80 nm and 450−500 nm, respectively. The EDS spectrum taken from the nanorods shows that the atomic composition ratio of Zn:O is about 1:1. However, the well-aligned characteristic was not observed as the ZnO nanorods grew on the sapphire (001). In contrast, the ZnO nanorods grown on the sapphire (110) substrate are not only oriented in *c*-axis direction but also form an orderly array in the *a*-axis direction. The diameter and the length of the ZnO nanorods grown on the sapphire (110) substrate were similar to those of the ZnO nanorods on the fused silica and the Si(100) substrates.

The crystal structure of the nanorods grown on various substrates was examined by XRD and TEM. As shown in Figure 2, in addition to the diffraction peaks of substrates, only the diffraction peaks of ZnO(002) and (004) appear in the XRD

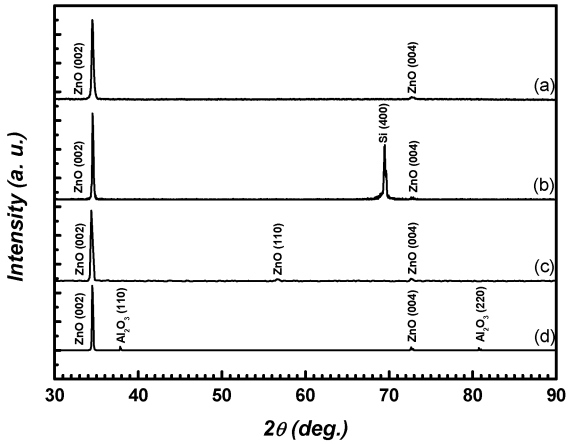

Figure 2. XRD spectra of ZnO nanorods grown on (a) fused silica, (b) Si(100), (c) sapphire (001), and (d) sapphire (110).

spectra of those grown on fused silica, Si(100), and sapphire (110), indicating that the ZnO nanorods on those substrates are preferentially oriented in the *c*-axis direction. The XRD spectrum of the ZnO nanorods grown on sapphire (001) shows that the diffraction peak of ZnO(110) appears in addition to (002) and (004) diffractions. Thus, the epitaxial relationship between ZnO and sapphire (001) substrate does not exist here as the SEM observation.

The cross-sectional TEM images of the ZnO nanorods grown on fused silica and Si(100) are shown in Figure 3a and b, respectively. They reveal that most of the nanorods were grown in a direction perpendicular to the fused silica and Si(100) substrates. The selection area diffraction (SAD) patterns of the cross-sectional images show discrete ring patterns, indicating that the nanorods are grown on fused silica and Si(100) randomly in the *a*-axis direction although they are preferentially oriented in the *c*-axis direction. In the ZnO nanorods grown on sapphire (110), as shown in Figure 4a, all of the ZnO nanorods grew in a direction perpendicular to the substrate. The SAD pattern taken from the ZnO nanorods of Figure 4a is shown in

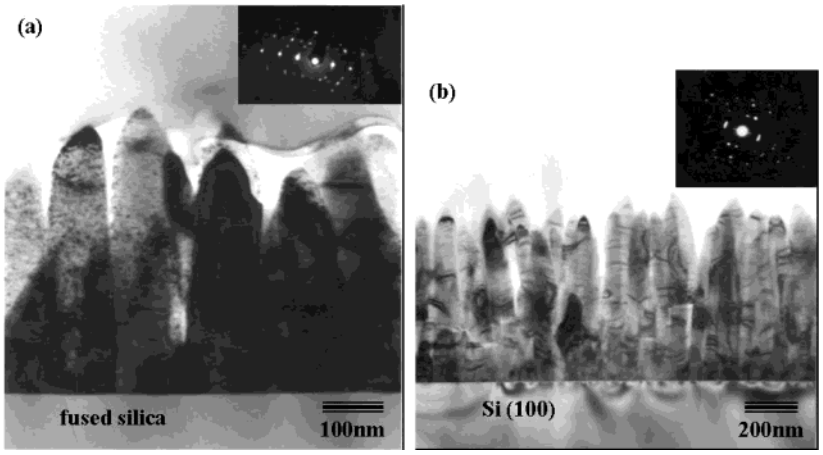

Figure 3. TEM cross-sectional images and SAD patterns (inset) of ZnO nanorods grown on (a) fused silica and (b) Si(100) substrate.

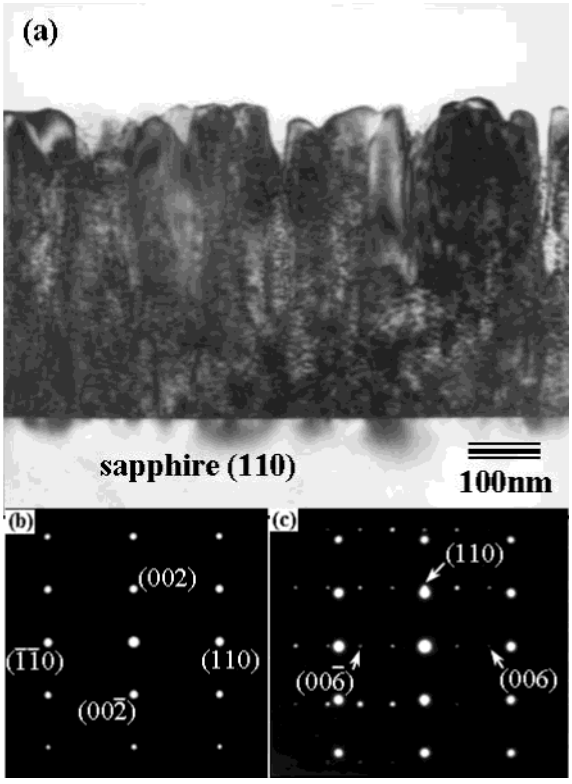

Figure 4. (a) TEM cross-sectional image of ZnO nanorods grown on sapphire (110) substrate, (b) SAD pattern of ZnO nanorods only in (a) with zone axis [1$\bar{1}$0], and (c) SAD pattern of ZnO nanorods and sapphire (110) substrate in (a) with zone axis [1$\bar{1}$0].

Figure 4b. In contrast to the discrete ring patterns from those grown on fused silica and Si(100) substrates, the single-crystal diffraction pattern indicates that the nanorods grown on sapphire (110) are oriented in both the *c*-axis and the *a*-axis directions. The SAD pattern taken from the interfacial region of the ZnO nanorods and sapphire (110) is shown in Figure 4c. It reveals that the ZnO nanorods possess an epitaxial relationship with the sapphire (110) substrate. With the zone axis of [1$\bar{1}$0] for both ZnO and Al_2O_3, the epitaxial relationship of ZnO nanorods and sapphire (110) substrate is identified: the [001] direction of ZnO nanorods aligns with the [110] direction of sapphire and the [110] direction of ZnO nanorods aligns with the [001] direction of sapphire.

To realize how the highly oriented ZnO nanorods and the epitaxial ZnO nanorods were grown on Si(100) and sapphire (110) substrates, respectively, HR-TEM was employed to study the interfacial regions of the ZnO nanorods and the two crystalline substrates. The HR-TEM image of the interfacial region of the ZnO nanorod and Si(100) substrate is shown in Figure 5a. It reveals that the ZnO(002) planes are parallel to Si(100) planes. Moreover, a 3-nm-thick amorphous layer exists between the ZnO nanorod and the Si substrate. EELS mapping analyses show the amorphous layer is composed of Si and O elements. Thus, a thin SiO_x amorphous layer was formed on the Si(100) first at a growth temperature of 500 °C, then ZnO nanorods were grown on the SiO_x layer preferentially in the *c*-axis direction. The HR-TEM image of the interfacial region of the ZnO nanorod and sapphire (110) substrate is shown in Figure 5b. The ZnO(002) planes are parallel to the sapphire (110) planes. A sharp interfacial transition from the sapphire to ZnO is observed between the two structures, indicating the epitaxial ZnO nanorod grown on sapphire (110) directly without any transition layer in-between.

Optical Characterization of ZnO Nanorods. Spectrum I in Figure 6a shows the room-temperature PL emission of the well-oriented ZnO nanorods grown on a fused silica substrate. Three emitting bands, including a strong ultraviolet emission at around 386 nm, a very weak blue band (440−480 nm), as well as an almost negligible green band (510−580 nm), are observed in the PL spectrum. Among them the UV emission must be the contribution of the near-band-edge emission of the wide band gap ZnO. It has been suggested that the green band emission corresponds to the singly ionized oxygen vacancy in ZnO.[10] Therefore, the almost negligible green band in this figure shows that there is a very low concentration of oxygen vacancy in the highly oriented ZnO nanorods. The absorption spectrum of the ZnO nanorods obtained at room temperature is shown in spectrum II of Figure 6a. The fundamental absorption of the semiconductor possessing allowed direct transitions can be determined by the energy dependence of[11]

$$\alpha(h\nu) \sim (h\nu - E_g)^{1/2}/h\nu$$

where α and E_g are the absorption coefficient and energy gap (at wave vector $k = 0$) of the semiconductor, respectively. Figure 6b presents the dependence of the absorption coefficient as a function of $h\nu$ (E) for the ZnO nanorods. The intercept defining the energy gap for the ZnO nanorods is 3.22 eV, which is consistent with the result of PL measurements.

The PL spectra of the ZnO nanorods on Si(100), sapphire (001), and sapphire (110) substrates are shown in Figure 7. The PL spectrum of the ZnO nanorods on Si(100) shows that only the UV near-band-edge emission peak appears. It reveals that

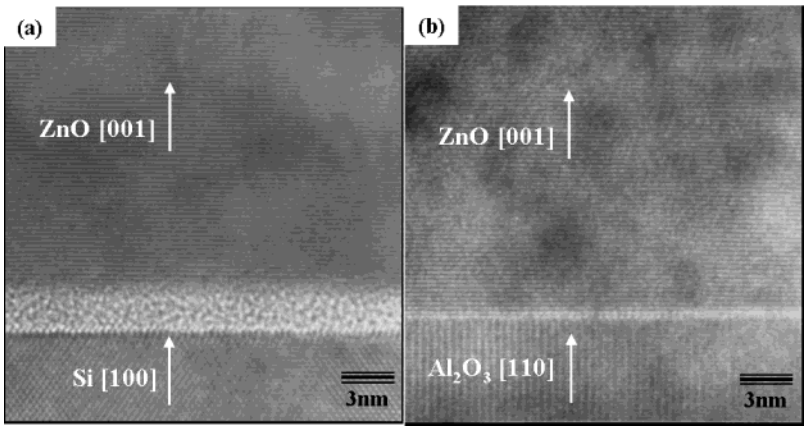

Figure 5. High-resolution TEM images of the interfacial regions of the ZnO nanorods and (a) Si(100) and (b) sapphire (110).

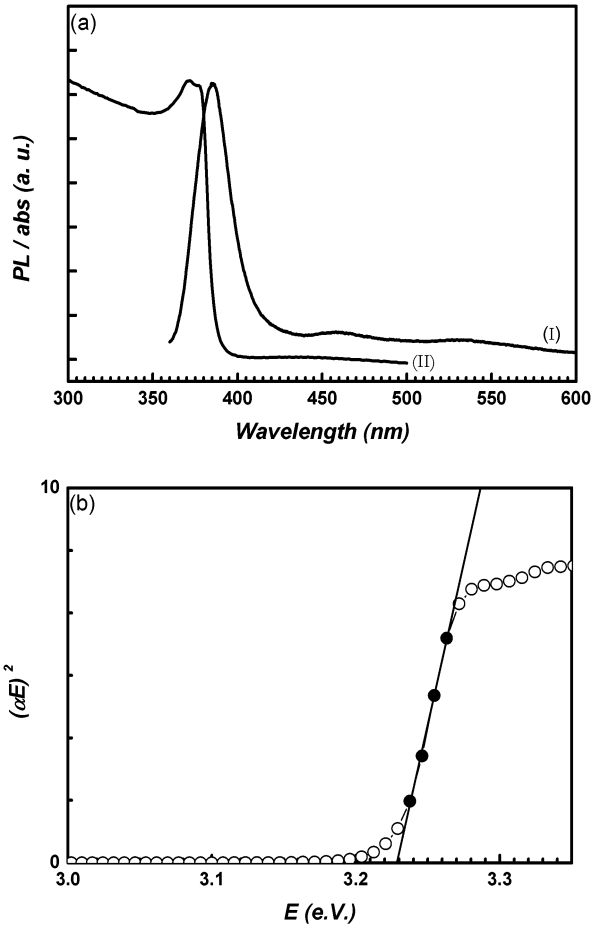

Figure 6. (a) Room-temperature photoluminescence (spectrum I) and absorption (spectrum II) spectra of ZnO nanorods on fused silica substrate. (b) Dependence of the absorption coefficient as a function of $h\nu$ for the ZnO nanorods.

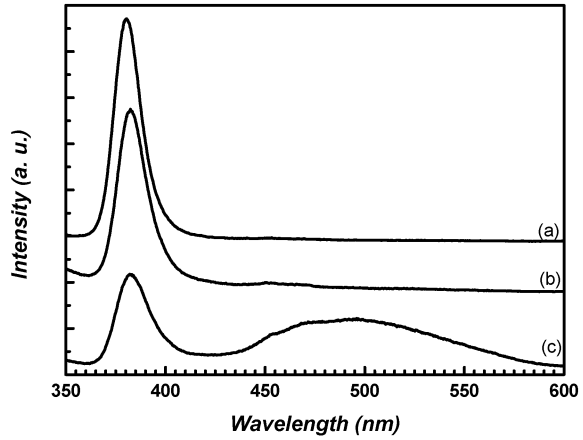

Figure 7. PL spectra of ZnO nanorods grown on (a) Si(100), (b) sapphire (001), and (c) sapphire (110).

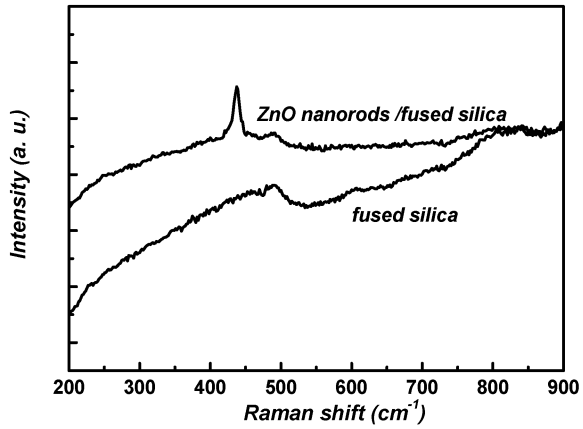

Figure 8. Raman spectra of the fused silica substrate and the ZnO nanorods on fused silica substrate.

the ZnO nanorods grown on the Si(100) exhibit a better quality than those grown on fused silica substrates. In the ZnO nanorods randomly grown on the sapphire (001), the PL spectrum also shows that only the UV emission band appears. However, the PL spectrum of the epitaxial ZnO nanorods on the sapphire (110) substrate shows that a broad green band appears in addition to the UV emission band, indicating a higher oxygen vacancy concentration in the ZnO nanorods grown on the sapphire (110) in comparison with those on the fused silica, Si(100), and sapphire (001). It is suspected that the oxygen vacancies were located in the interfacial region of the ZnO nanorods and sapphire (110) because of lattice mismatch between them, leading to the green band emission of the epitaxial ZnO nanorods.

The Raman spectra of the fused silica substrate and the highly oriented ZnO nanorods grown on fused silica substrate are both shown in Figure 8. In comparison with a bare fused silica substrate, only a peak at 437 cm^{-1} corresponding to the E_2 mode of ZnO crystal is the contribution of the ZnO nanorods. The absence of the E_1 (LO) mode of ZnO crystal at 583 cm^{-1}, which is associated with oxygen deficiency,[12] reveals the high quality of the ZnO nanorods, as does the negligible green band in the PL spectrum.

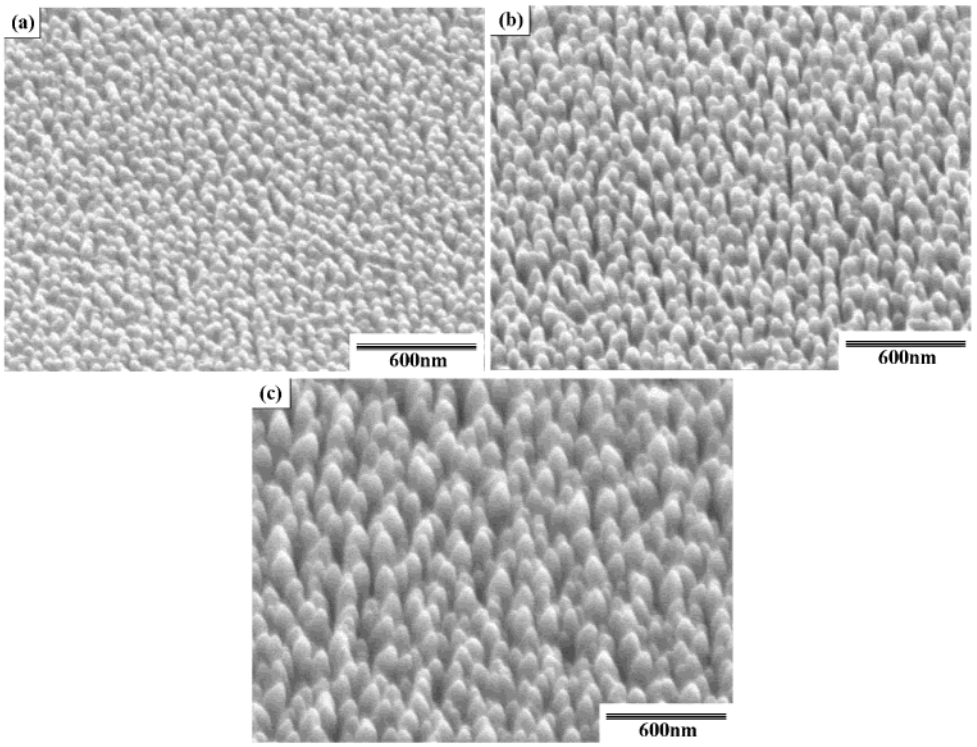

Figure 9. SEM images of ZnO nanorods with various average diameters (a) 45 nm, (b) 60 nm, and (c) 90 nm.

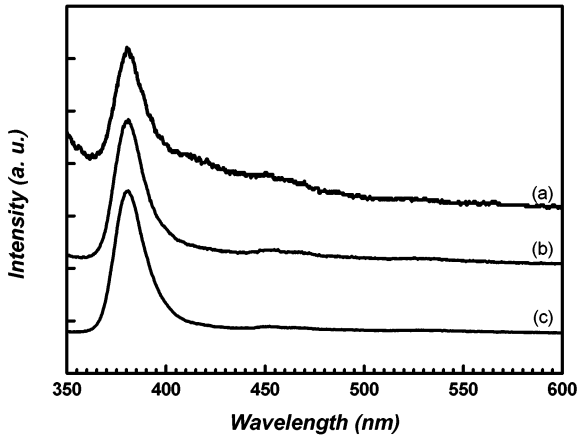

Figure 10. PL spectra of the ZnO nanorods shown in Figure 9.

Diameter-Controlled Growth of the Highly Oriented ZnO Nanorods. The highly oriented ZnO nanorods on fused silica substrates with various average diameters were synthesized using the catalyst-free CVD method by adjusting the growth conditions, such as the vapor flux of the zinc source, the substrate temperature, the N_2/O_2 flow rates, and so forth. Figure 9 demonstrates the case of control of the diameters of the ZnO nanorods by variation of the vapor flux of the zinc source. Syntheses of ZnO nanorods on fused silica substrates with average diameters of 45, 60, and 90 nm are achieved by use of zinc source containers with various open areas at vaporizing temperatures of 135−138 °C, a N_2/O_2 flow rate of 500/250 sccm, and a substrate temperature of 500 °C. The average lengths of the ZnO nanorods shown in Figure 9a−c are all 250 nm. Their PL spectra are shown in Figure 10. All of them possess a strong UV emission peak, a very weak blue band, as well as an almost negligible green band. Therefore, diameter-controlled growth of the ZnO nanorods on fused silica substrate with good quality is achievable by adjusting the vapor flux of the zinc source using the low-temperature CVD approach. In addition, the diameter of the ZnO nanorods can be reduced as the vaporizing temperature of the zinc source increases while it is getting larger as the substrate temperature increases under the following condition ranges: source vaporizing temperature, substrate temperature, N_2/O_2 flow rates from 130 °C to 138 °C, 450 °C to 550 °C, and 250/250 to 750/250 sccm, respectively. PL measurements reveal that all the ZnO nanorods synthesized under the conditions mentioned above possess a strong UV near-band-edge emission.

Mechanism of the ZnO Nanorod Growth. There are two well-accepted mechanisms for 1-D material growth: the VLS mechanism and the screw dislocation mechanism.[13] In the VLS mechanism, metallic particles which play a role as catalysts for the formation of 1-D structures commonly remained at the end of the 1-D structures. In this study, no additional metal particle appeared on the top or the bottom of the nanorods, as shown in SEM and TEM images, implying a non-VLS approach to growth of the well-aligned ZnO nanorods was achieved. On the other hand, a conic tip with spiral morphology at the end of the 1-D structured material, resulting from the existence of a screw dislocation whose line is parallel to the axis of the 1-D structures, is the evidence for 1-D material growth by the screw dislocation mechanism. The spiral plane perpendicular to the screw dislocation line possesses a step as a low-energy site for growth. The growth rate along the dislocation line is then much faster than that of radius direction which results in the crystal with 1-D structured morphology. However, as shown in Figure 11, instead of spiral morphology at the tip, well-faceted prismatic morphology is observed on the tops of the ZnO nanorods, indicating that the growth of the ZnO nanorods did not follow the screw dislocation mechanism in this study. A possible mechanism for the ZnO nanorod growth is proposed as follows. The growth habit of crystals is related to the relative growth rate of various crystal faces bounding the crystal, which is mainly determined by the internal structure of a given crystal as well as is affected by growth conditions.[14] The direction of the crystal face with the corner of the coordination polyhedron occurring at the

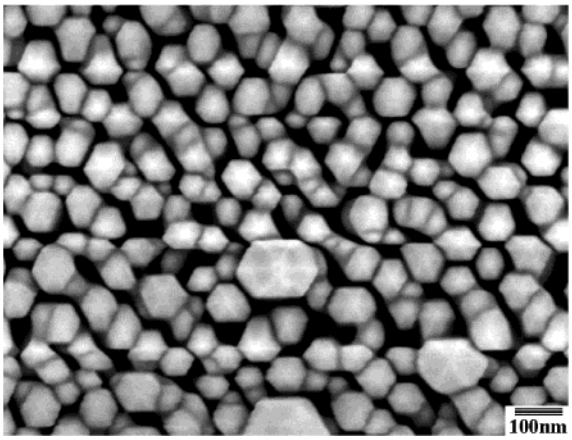

Figure 11. High-resolution SEM images of the ZnO nanorods grown on the sapphire (110) substrate.

interface possesses the fastest growth rate, and the directions of the crystal face with the edge and with the face of the coordination polyhedron occurring at the interface have the second fastest and the slowest growth rates, respectively.[14] Figure 1d and Figure 11 suggest that the relationship of the growth rates (R) of the ZnO crystal faces is $R_{<001>} > R_{<101>} > R_{<100>}$, resulting in the formation of the 1-D ZnO nanorods with prismatic morphology on the tops. The aspect ratios of the ZnO nanorods are determined by the relative growth rate of these crystal faces, which is adjustable by growth conditions in this study. Therefore, diameter-controlled growth of the ZnO nanorods was achieved as shown in Figure 9.

In contrast to the 1-D single-crystalline ZnO nanostructures synthesized by various high-temperature methods,[5,6] the growth of high-quality ZnO films are able to be performed at lower temperatures ranging from 450 °C to 750 °C using techniques such as molecular beam eptiaxy (MBE),[4] metalorganic chemical vapor deposition (MOCVD),[15] pulsed laser depsoition,[16] and so forth. In this study, the chemical mechanism of the 1-D ZnO nanorods growth at low temperatures using zinc acetylacetonate and O_2 in the absence of catalyst is suggested to be similar to that of the ZnO films deposited using MOCVD. Although there are four oxygen atoms per zinc acetylacetonate molecule, the addition of O_2 is still necessary for the growth of the ZnO nanorods. Zinc acetylactonate possesses a low melting (decomposed) temperature at around 138 °C. Mass spectrometry study has demonstrated that the major species of the zinc acetylacetonate vapor at temperatures of 130−200 °C are $(CH_3COCH{=}C(O-)CH_3)Zn(COCH{=}C(O-)CH_3)$, $(CH_3COCH{=}C(O-)CH_3)Zn(CH_2{=}C(O-))$, $(CH_3COCH{=}C(O-)CH_3)Zn$ and Zn, in addition to zinc acetylacetonate itself.[17] Some of these active zinc species which were formed in the gas phase of the furnace at temperatures ranging from 130 °C to 500 °C could be the Zn precursors reacting with oxygen on the surface for the ZnO nanorod growth.

Conclusions

Highly oriented ZnO nanorods have been grown on fused silica and Si(100) substrates using a simple catalyst-free CVD method at low temperatures. An amorphous SiO_x layer is observed from the HRTEM image in the interface of ZnO nanorods and Si(100). The highly oriented ZnO nanorods exhibit a strong UV emission of 386 nm at room temperature. Photoluminescence and Raman spectra indicate that there is a very low concentration of oxygen vacancies in the highly oriented ZnO nanorods. Epitaxial ZnO nanorods have been grown on sapphire (110) with the ZnO/sapphire orientational relationship [001]||[110] and [110]||[001]. Furthermore, diameter control of the well-aligned and high-quality ZnO nanorods on fused silica substrates is achievable by varying the growth conditions. We believe the presented approach is a simple one for practical application of ZnO nanostructures to optoelectronic devices.

Acknowledgment. The authors would like to thank Prof. Y. Chen, Dr. K. H. Chen, Dr. L. C. Chen, and Dr. X. J. Guo for help on PL, Raman, HRSEM, and TEM measurements, respectively. The financial support of this work, by the National Science Council in Taiwan under Contract No. NSC 89-2214-E-006-023, is gratefully acknowledged.

References and Notes

(1) (a) Lieber, C. M. *Solid State Commun.* **1998**, *107*, 607−616. (b) Hu, J.; Odom, T. W.; Liber, C. M. *Acc. Chem. Res.* **1999**, *32*, 435−445.

(2) (a) King, D. S.; Nix, R. M. *J. Catal.* **1996**, *160*, 76−83. (b) Minami, T. *Mater. Res. Soc. Bull.* **2000**, *25*, 38−44. (c) Bagnall, D. M.; Chen, Y. F.; Zhu, Z.; Yao, T.; Koyama, S.; Shen, M. Y.; Goto, T. *Appl. Phys. Lett.* **1997**, *70*, 2230−2232. (d) Zhong, J.; Kitai, A. H.; Mascher, P.; Puff, W. *J. Electrochem. Soc.* **1993**, *140*, 3644−3649.

(3) (a) Bagnall, D. M.; Chen, Y. F.; Zhu, Z.; Yao, T.; Koyama, S.; Shen, M. Y.; Goto, T. *Appl. Phys. Lett.* **1997**, *70*, 2230−2232. (b) Zu, P.; Tang, Z. K.; Wong, G. K. L.; Kawasaki, M.; Ohtomo, A.; Koinuma, H.; Segawa, Y. *Solid State Commun.* **1997**, *103*, 459−463. (c) Co, H.; Xu, J. Y.; Seelig, E. W.; Chang, R. P. H. *Appl. Phys. Lett.* **2000**, *76*, 2997−2999.

(4) (a) Chen, Y.; Bagnall, D. M.; Koh, H.; Park, K.; Hiraga, K.; Zhu, Z.; Yao, T. *J. Appl. Phys.* **1998**, *84*, 3912−3918. (b) Ohtomo, A.; Kawasaki, M.; Sakurai, Y.; Ohkubo, I.; Shiroki, R.; Yoshida, Y.; Yasuda, T.; Segawa, Y.; Koinuma, H. *Mater. Sci. Eng., B* **1998**, *56*, 263−266.

(5) (a) Huang, M. H.; Wu, Y.; Feick, H.; Tran, N.; Weber, E.; Yang, P. *Adv. Mater.* **2001**, *13*, 113−116. (b) Kong, Y. C.; Yu, D. P.; Zhang, B.; Fang, W.; Feng, S. Q. *Appl. Phys. Lett.* **2001**, *78*, 407−409.

(6) Pan, Z. W.; Dai, Z. R.; Wang, Z. L. *Science* **2001**, *291*, 1947−1949.

(7) (a) Huang, M. H.; Mao, S.; Feick, H.; Yan, H.; Wu, Y.; Kind, H.; Weber, E.; Russo, R.; Yang, P. *Science* **2001**, *292*, 1897−1899. (b) Johnson, J. C.; Yan, H.; Schaller, R.; Haber, L. H.; Saykally, R. J.; Yang, P. *J. Phys. Chem.* **2001**, *105*, 11387−11390.

(8) Wu, J.-J.; Liu, S.-C. *Adv. Mater.* **2002**, *14*, 215−218.

(9) (a) Chen, Y.; Bagnall, D. M.; Koh, H.; Park, K.; Hiraga, K.; Zhu, Z.; Yao, T. *J. Appl. Phys.* **1998**, *84*, 3912−3918. (b) Fons, P.; Iwata, K.; Yamada, A.; Matsubara, K.; Niki, S.; Nakahara, K.; Tanabe, T.; Takasu, H. *Appl. Phys. Lett.* **2000**, *77*, 1801−1803.

(10) Vanheusden, K.; Warren, W. L.; Seager, C. H.; Tallant, D. R.; Voigt, J. A.; Gnade, B. E. *J. Appl. Phys.* **1996**, *79*, 7983−7990.

(11) Pankove, J. I. *Optical Processes in Semiconductors*; Prentice Hall: NJ, 1971.

(12) (a) Xu, X. L.; Lau, S. P.; Chen, J. S.; Chen, G. Y.; Tay, B. K. *J. Cryst. Growth* **2001**, *223*, 201−205. (b) Exarhos, G. J.; Sharma, S. K. *Thin Solid Films* **1995**, *270*, 27−32.

(13) (a) Wang, L.; Wada, H.; Allard, L. F. *J. Mater. Res.* **1992**, *7*, 148−163. (b) Sear, G. W. *Acta Metall.* **1953**, *1*, 457−459. (c) Wagner, R. S.; Ellis, W. C. *Appl. Phys. Lett.* **1964**, *4*, 89−90.

(14) (a) Laudise, R. A.; Ballman, A. A. *J. Phys. Chem.* **1960**, *64*, 688−691. (b) Li, W.-J.; Shi, E.-W.; Zhong, W.-Z.; Yin, Z.-W. *J. Cryst. Growth* **1999**, 186−196.

(15) (a) Gorla, C. R.; Emanetoglu, N. W.; Liang, S.; Mayo, W. E.; Lu, Y.; Wraback, M.; Shen, H. *J. Appl. Phys.* **1999**, *85*, 2595−2602. (b) Kashiwaba, Y.; Haga, K.; Watanabe, H.; Zhang, B. P.; Segawa, Y.; Wakatsuki, K. *Phys. Status Solidi B* **2002**, *229*, 921−924.

(16) (a) Joseph, M.; Tabata, H.; Kawai, T. *Jpn. J. Appl. Phys.* **1999**, 38, L1205−L1207. (b) Guo, X.; Choi, J.; Tabata, H.; Kawai, T. *Jpn. J. Appl. Phys.* **2001**, *40*, L117−L180.

(17) Macdonald, C. G.; Shannon, J. S. *Aust. J. Chem.* **1966**, *19*, 1545−1566.